Proceedings of BS2013:
13th Conference of International Building Performance Simulation Association, Chambéry, France, August 26-28

CFD SIMULATION OF TEMPERATURE STRATIFICATION FOR A BUILDING SPACE: VALIDATION AND SENSITIVITY ANALYSIS

S. Gilani[1], H. Montazeri[2], B. Blocken[2]

[1]School of Architecture, University of Tehran, Tehran, Iran
[2]Building Physics and Services, Eindhoven University of Technology, Eindhoven, The Netherlands

ABSTRACT

Accurate and reliable CFD simulation of temperature stratification in indoor environment is needed for the design and evaluation of displacement ventilation in buildings. This paper presents a detailed and systematic evaluation of the capability of 3D steady RANS CFD simulations to predict the temperature stratification in a room. The evaluation is based on sensitivity analysis and validation with full-scale measurements of indoor air temperature. The results show that steady RANS can accurately predict the temperature stratification in an indoor environment. The SST *k-ω* model shows a better performance compared with other considered turbulence models.

INTRODUCTION

Temperature stratification generated by heat sources such as heating systems, occupants, electronic equipment, and solar radiation on interior surfaces is the common feature of the buoyancy-driven ventilation called displacement ventilation. This mode of ventilation can efficiently purge excess heat and pollutants from interior spaces. Therefore, knowledge of the temperature stratification in building spaces is required to improve occupants' thermal comfort and indoor air quality. In addition, it can be incorporated into more appropriate designs for higher interior spaces like atriums.

Investigation of the vertical temperature distribution in enclosed spaces can be performed by different methods: full-scale experiments (Saïd et al., 1996; Xu et al., 2001; Wan and Chao, 2005; Crouzeix et al., 2006b; Awad et al., 2008), reduced-scale experiments (Cooper and Linden, 1996; Tovar et al., 2007), analytical methods (Nielsen, 1979; Li et al., 1992; Cooper and Linden, 1996; Li, 2000; Crouzeix et al., 2006a), and numerical simulation with Computational Fluid Dynamics (CFD) (Wan and Chao, 2005; Stamou and Katsiris, 2006). CFD can be used as quite a more efficient tool in comparison with the other methods (Linden, 1999; van Hooff and Blocken, 2010; Blocken et al., 2011). The main advantage of CFD is that it can provide detailed flow data in the whole computational domain. CFD is not concerned with similarity constraints due to its potential for full-scale simulations. Parametric studies can be carried out easily and efficiently by using CFD. In addition, the application of CFD for studying indoor air quality (e.g. Hayashi et al., 2002), natural ventilation (e.g. Gao and Lee, 2011; Bangalee et al., 2012; Ramponi and Blocken, 2012), and stratified indoor environment (e.g. Howell and Potts, 2002) are extensively increasing since these are difficult to be predicted with other methods (Chen, 2009). Despite all the mentioned advantages, the accuracy and reliability of CFD simulation are its main concerns. Therefore, CFD validation and verification are imperative.

This paper presents a detailed sensitivity analysis of 3D steady RANS CFD simulations to predict the temperature stratification in a room with a heat source and two ventilation openings. The CFD simulations are validated based on full-scale measurements of the indoor air temperature by Li et al. (1992, 1993). The effects of different turbulence models, the computational grid resolution, the discretization scheme, and the iterative convergence are analyzed.

First, the full-scale measurements of indoor air temperature by Li et al. (1992, 1993) are briefly described. Then, the computational settings and parameters for the reference case are explained and the results of the CFD simulation are compared with the experiment. Afterwards, the sensitivity analysis is performed. At last, the limitations of the study are discussed and finally the main conclusions are outlined.

DESCRIPTION OF FULL-SCALE EXPERIMENT

Temperature measurements of a typical room projected to displacement ventilation were performed by Li et al. (1992, 1993) in the Heating and Ventilation Laboratory of the National Swedish Institute for Building Research. The test-room was a full-scale model with dimensions width × length ×

height = 3.6 × 4.2 × 2.75 m^3 (Figure 1). All the interior surfaces of the test-room walls were painted black or covered with aluminum sheets. The overall heat transfer coefficients (U-values) of all the test-room walls, including floor, ceiling, and vertical walls except wall 4 were 0.36 $W/m^2.K$. The U-value of wall 4 was 0.15 $W/m^2.K$. The air was supplied into the test-room through an inlet at floor level. It had dimensions 0.45 × 0.5 m^2 and 50 % of its area was perforated that resulted in 0.1125 m^2 as the total opening area of the inlet. The air was extracted from the test-room through an outlet with dimensions of 0.525 × 0.220 m^2 that was located at height of 2.39 m in wall 2. A heat source with the dimensions 0.3 × 0.4 × 0.3 m^3 induced displacement ventilation in the test-room. It was placed 0.1 m above floor level, 2.7 m from the inlet, and in the center of the room length (Figure 1). It incorporated 24 light bulbs of 25 W in an aluminum cube, providing heat loads up to 600 W.

The air temperature was measured by means of 30 thermocouples located along one vertical pole inside the test-room (Figure 1). Most of the thermocouples were concentrated near the floor and the ceiling. The interior surface temperature of the test-room was measured by 22 thermocouples, five on each wall, one on the ceiling, and one on the floor. Two thermocouples measured inlet and outlet air temperatures. Five thermocouples also measured the exterior surface temperature of the walls and the ceiling. The measurement uncertainty was estimated to be ±0.1 °C.

In this experiment, the impacts of different parameters such as heat load, wall emissivity, inlet flow rate, and inlet air temperature were investigated. The focus of the present paper is on the case with the black-painted walls and one air change per hour (n). The inlet (T_i) and the outlet air temperature (T_o) were 289.15 K and 300.45 K respectively. The heat load (E) in this case was 300 W.

CFD SIMULATIONS: REFERENCE CASE

In this section, the computational grid, boundary conditions, and solver settings for the reference case are described. This case was used as a reference for comparing the results of the sensitivity analysis.

Computational grid

A computational model was made of the room used in the full-scale measurement. The computational grid of the reference case had 451,248 hexahedral cells generated using the surface-grid extrusion method presented by van Hooff and Blocken (2010) (Figure 2). The maximum stretching ratio was 1.2. A total number of 6 and 25 cells were used along the length and the height of the inlet. 8 and 7 cells were used along the length and the height of the outlet. The distance from the centre point of the wall-adjacent cell to the wall for different surfaces of the room was 0.0005 m. This corresponds to y^* values between 0.007 and 1.801. As low-Reynolds number models were used in this study, this value ensured that a few cells were placed in the viscous sublayer. The viscous sublayer thickness was assumed to be 0.04 m and at least 10 cells were positioned in this region ($Re_y < 200$) (ANSYS, 2009).

Boundary conditions

The heat source inside the test-room was defined as an energy source term with a constant heat generation of about 8333 W/m^3 according to Equation 1:

$$q = \frac{E}{V_{hs}} \quad (1)$$

where q is the volumetric heat generation (W/m^3), E is the heat load (W), and V_{hs} is the heat source volume (m^3).

The incompressible ideal gas law was used to estimate the air density as a function of T (ANSYS, 2009). Other air properties were determined according to the average value of the measured air temperatures along the vertical pole inside the test-room (297.69 K). In this case, the Prandtl number of the air was 0.71. The operating pressure and operating density were 101325 Pa and 1.172 kg/m^3 respectively (Bergman et al., 2011). At the test-room outlet, zero static pressure was specified.

The inlet condition was a constant velocity which was calculated based on the experimental data and by using Equation 2:

$$u = \frac{Q}{A_i} = \frac{nV}{A_i} \quad (2)$$

where u is the inlet air velocity (m/s), Q is the inlet flow rate (m^3/s), A_i is the inlet opening area (m^2), n is the number of test-room air change (1/s), and V is the test-room volume (m^3). The inlet air temperature (T_i) was 289.15 K according to the experimental data.

A fixed temperature condition was applied for the test-room walls, including the vertical walls, the floor, and the ceiling. In the experiment, the average values of the interior surface temperatures of the four vertical walls were provided at five different heights (Table 1). The same values were used as the thermal boundary conditions of the vertical walls in the CFD simulations. For this purpose, the interior surface temperature at different heights of the vertical walls were defined by user-defined functions (UDFs) (Table 2).

Although the interior surface temperature of the floor and the ceiling were measured in the experiment, their values were not mentioned in the paper by Li et al. (1993). Therefore, in the present paper, the interior surface temperature of the floor and the

ceiling were calculated based on the following explanation.

The floor surface temperature (T_{if}) (296.98 K) was calculated using Equation 3 (Li et al., 1992):

$$T_{if} = \frac{\rho\, c_p\, Q\, (T_f^a - T_i)}{h_i\, A_f} + T_f^a \qquad (3)$$

where ρ is the air density (kg/m^3), c_p is the specific heat capacity of air (J/kg.K), Q is the inlet flow rate (m^3/s), T_f^a is the near-floor air temperature (295.93 K), T_i is the inlet air temperature (K), h_i is the interior convective heat transfer coefficient (5.88 W/m^2.K) (ISO, 2007), and A_f is the floor surface area (m^2).

Interior surface temperature of the ceiling (T_{ic}) was calculated by applying the energy conservation equation at the control surface assumed to be on either side of the interior surface of the ceiling. There are three heat transfer mechanisms for this control surface: conduction from the medium to the control surface (q''_{cond}), convection from the surface to a fluid (q''_{conv}), and radiation from the surface to the surroundings (q''_{rad}) as explained by Bergman et al. (2011) in Equations 4 and 5:

$$q''_{cond} = q''_{conv} + q''_{rad} \qquad (4)$$

$$\frac{k}{L}\,(T_{ec} - T_{ic}) = h_i(T_{ic} - T_\infty) + \sigma\varepsilon_i(T_{ic}^4 - T_{sur}^4) \qquad (5)$$

where k is the thermal conductivity of the ceiling material (W/m.K), L is the ceiling thickness (m), T_{ec} is the exterior surface temperature of the ceiling (293.45 K), T_{ic} is the interior surface temperature of the ceiling (K), h_i is the interior convective heat transfer coefficient (10 W/m^2.K) (ISO, 2007), T_∞ is the ambient air temperature (K), σ is Stefan-Boltzmann constant (W/m^2.K^4), ε_i is the surface emissivity, and T_{sur} is the temperature of the surroundings (K). It needs to be noted that it was assumed that the radiation exchange occurred only between the ceiling and the floor (Li et al., 1992, 1993). Therefore, in Equation 5, T_{sur} would be the floor surface temperature (T_{if}).

Proportion of the thermal conductivity of the ceiling to its thickness (K/L) was obtained 0.388 W/m^2.K based on Equation 6:

$$\frac{1}{U} = \frac{1}{h_e} + \frac{L}{k} + \frac{1}{h_i} \qquad (6)$$

where U is the overall heat transfer coefficient (W/m^2.K), h_e is the exterior convective heat transfer coefficient (10 W/m^2.K), L is the ceiling thickness (m), k is the thermal conductivity of ceiling material (W/m.K), and h_i is the interior convective heat transfer coefficient (10 W/m^2.K).

So, by knowing all the parameters in Equation 5, the interior surface temperature of the ceiling was obtained 297.33 K.

Solver settings

The commercial CFD code Fluent 12.1 was used to perform the simulations (ANSYS, 2009). The 3D steady RANS equations were solved in combination with the Shear-Stress Transport (SST) k-ω model (Menter, 1994). The SIMPLE algorithm was used for pressure-velocity coupling. Second order discretization schemes were used for both the convection terms and the viscous terms of the governing equations. PRESTO! scheme was applied for the pressure terms. Because of the temperature-dependent density of the air, the energy and momentum equations were solved simultaneously.

Results and comparison with experiment

The CFD results for the reference case are compared with the full-scale measurements by Li et al. (1993). The difference between the air temperature (T) and the inlet air temperature (T_i) is given as the temperature difference. Figure 3a shows the CFD results and the experimental results along the vertical pole inside the test-room. Figure 3b also gives the absolute deviation between the CFD results and the experimental results. The general agreement between the CFD simulation and the experiment is quite good. Note that CFD underestimates the temperature near the floor and the ceiling and overestimates it at the other parts of the pole. The average and maximum absolute deviation of temperature difference between the CFD simulation results and the measurements are 4.42% and 13.46% respectively.

Figure 4a and b show the air temperature distribution and Figure 4c and d show the velocity vector field across two vertical planes located 2.7 m from wall 1 and 2.1 m from wall 2. These figures show that the plume-type flow generated above the heat source causes a recirculation flow below the ceiling. In this way, the temperature stratification phenomenon is developed outside the plume that resembles the displacement ventilation.

CFD SIMULATION: SENSITIVITY ANALYSIS

In this section, the impacts of different computational parameters are analyzed in detail. For this purpose, a single parameter is altered systematically in every stage and its impact on the simulation results is compared with the reference case described in the previous section.

Impact of computational grid resolution

Two grids other than the reference grid with 451,248 cells were made: a finer grid and a coarser gird. Refining and coarsening were performed with an overall linear factor √2. The coarser grid had 155,382 cells and the finer grid had 1,268,736 cells. The three generated grids are shown in Figure 5. The temperature difference along the vertical pole for the

three grids is shown in Figure 6a. The average absolute deviations between the CFD simulation results and the measurements are 4.61%, 4.42%, and 4.20% for the coarse, reference, and fine grid respectively. In addition, the maximum absolute deviations between the CFD simulation results and the measurements are 13.64%, 13.46%, and 13.41% for the coarse, reference, and fine grid respectively. The method of Grid-Convergence Index (GCI) by Roache (1994, 1997) was used for uniform reporting of grid convergence study (Figure 6b). The results show that the deviation is more noticeable in the lower part of the pole. For the other parts of the pole, the deviation is negligible. Therefore, the reference grid is retained for further analysis.

Impact of turbulence model

3D steady CFD simulations were performed with different Reynolds-Averaged Navier-Stokes (RANS) turbulence models including:

- Standard k-ε model (Sk-ε) (Launder and Spalding, 1972),
- Realizable k-ε model (Rk-ε) (Shih et al., 1995),
- Renormalization Group k-ε model (RNG k-ε) (Yakhot and Orszag, 1986),
- Standard k-ω model (Sk-ω) (Wilcox, 1998), and
- Shear-stress transport (SST) k-ω model (SST k-ω) (Menter, 1994).

Note that the Sk-ε, Rk-ε, and the RNG k-ε model were used in combination with the low-Re number Wolfshtein model (1969). The impact of turbulence models on the CFD simulation results of the temperature difference along the vertical pole is illustrated in Figure 7. The differences between the models are considerable along the pole except near the ceiling. All the models tend to overestimate the temperature in the middle of the pole and underestimate it near the ceiling. In addition, all the models, except the RNG k-ε, underestimate the temperature near the floor.

The average absolute deviations between the CFD simulation results and the measurements for the Sk-ε, Rk-ε, RNG k-ε, Sk-ω, and the SST k-ω are 6.56%, 6.40%, 6.77%, 5.19%, and 4.42% respectively. It can be seen that the SST k-ω model shows the best performance compared with the considered models. This has been mentioned in several previous studies (e.g. Stamou and Katsiris, 2006; Hussain and Oosthuizen, 2012; Hussain et al., 2012; Ramponi and Blocken, 2012).

Impact of order of discretization scheme

The impact of discretization scheme on the temperature difference along the vertical pole is shown in Figure 8. The discrepancies between the first-order and the second-order discretization scheme are more prominent near the ceiling. The average absolute deviations are 5.10% and 4.42% for the first-order and the second-order discretization scheme respectively.

Impact of level of iterative convergence

In this study, three criteria were employed simultaneously to decide on whether a converged solution was obtained or not. First, the scaled residuals decreased to at least 10^{-3} for all equations except the energy equation for which the residual of at least 10^{-6} was obtained. Second, the net imbalance of the heat flow rate was less than 1% of the smallest heat flow rate through the domain boundary. Third, some key flow variables were checked to see whether a constant value was obtained for them.

The impact of the iterative convergence limit on the temperature difference along the vertical pole is shown in Figure 9. It can be observed that the criterion of just 10^{-3} for the scaled residuals is not sufficient for this situation and further iterations are necessary to reach a converged solution that is in good agreement with the experiment measurements. The average absolute deviations from the measurements are 4.68% and 4.47% for the 10^{-3} and 10^{-4} level respectively. It needs to be noted that in Figure 9 just the first mentioned criterion was considered for both 10^{-3} and 10^{-4}. In other words, for 10^{-3} it was assumed that a converged solution was achieved if the scaled residuals decreased to 10^{-3} for all equations except the energy equation for which the residual of at least 10^{-6} was acceptable. In addition, for 10^{-4} it was assumed that a converged solution was obtained if the scaled residuals decreased to 10^{-4} for all equations except the energy equation for which the residual of at least 10^{-6} was acceptable.

DISCUSSION

It is important to mention some limitations of this study:

- In this study, steady RANS CFD simulations were performed for a one-storey building space with a heat source and two ventilation openings. A parametric analysis still needs to be performed to investigate the effect of interior space geometry, location of the heat source, number of room air changes, different heat loads, and number, location, and size of the ventilation openings.
- This study was performed for a single isolated building space and the influence of connected interior spaces was not investigated. Further research is needed on the validation, verification and sensitivity analysis of steady RANS CFD simulation for the temperature stratification in more complex spaces.
- The study was performed in combination with the steady RANS models. The performance of transient CFD simulations with DES and LES still need to be evaluated for the temperature stratification in indoor spaces.

• Further research is necessary on exploring the impact of radiative heat transfer between the interior surfaces and conductive heat transfer through the walls.

CONCLUSIONS

Knowledge of temperature stratification in indoor environment can lead to more efficient performance and control of displacement ventilation, thereby reducing the need for air conditioning systems and developing healthy indoor environments. In this study, a detailed assessment of 3D steady RANS CFD simulations for the prediction of temperature stratification in a room was performed. This study was based on sensitivity analysis and validation with full-scale measurements.

This study confirmed that the steady RANS CFD simulation has the capability of demonstrating the main features of temperature stratification in indoor environment. The general agreement between the CFD simulation and the experiment was satisfactory. The grid sensitivity analysis showed that the lower part of the room is more sensitive to the computational grid resolution. Concerning the turbulence models, the SST k-ω model showed the more reliable results in comparison with other considered turbulence models. Finally, stricter convergence criteria were needed for obtaining more accurate CFD simulation results.

NOMENCLATURE

σ = Stefan-Boltzmann constant
ε_i = surface emissivity
T_f^a = near-floor air temperature
A_f = floor surface area
A_i = inlet opening area
c_p = specific heat capacity of air
E = heat load
h_e = exterior convective heat transfer coefficient
h_i = interior convective heat transfer coefficient
k = thermal conductivity
L = thickness
n = number of test-room air change
Q = inlet flow rate
q = volumetric heat generation
T_∞ = ambient air temperature
T_{ec} = exterior surface temperature of the ceiling
T_i = inlet air temperature
T_{ic} = interior surface temperature of the ceiling
T_{if} = floor surface temperature
T_o = outlet air temperature
T_{sur} = surroundings temperature
u = inlet air velocity
U = overall heat transfer coefficient
V = test-room volume
V_{hs} = heat source volume
ρ = air density

ACKNOWLEDGEMENTS

The authors would like to express their thankfulness to the technical members of the Laboratory of the Unit Building Physics and Services at the Eindhoven University of Technology for the important computing infrastructure support.

REFERENCES

ANSYS. 2009. ANSYS Fluent 12.0 user's guide: ANSYS, Inc.

Awad AS, Calay RK, Badran OO, Holdo AE. 2008. An experimental study of stratified flow in enclosures. Applied Thermal Engineering 28:2150-2158.

Bangalee MZI, Lin SY, Miau JJ. 2012. Wind driven natural ventilation through multiple windows of a building: A computational approach. Energy and Buildings 45:317-325.

Bergman TL, Lavine AS, Incropera FP, Dewitt DP. 2011. Fundamentals of heat and mass transfer, Seventh ed: John Wiley and Sons, Inc.

Blocken B, Stathopoulos T, Carmeliet J, Hensen JLM. 2011. Application of computational fluid dynamics in building performance simulation for the outdoor environment: An overview. Journal of Building Performance Simulation 4:157-184.

Chen Q. 2009. Ventilation performance prediction for buildings: A method overview and recent applications. Building and Environment 44:848-858.

Cooper P, Linden PF. 1996. Natural ventilation of an enclosure containing two buoyancy sources. Journal of Fluid Mechanics 311:153-176.

Crouzeix C, Le Mouël JL, Perrier F, Richon P. 2006a. Non-adiabatic boundaries and thermal stratification in a confined volume. International Journal of Heat and Mass Transfer 49:1974-1980.

Crouzeix C, Le Mouël JL, Perrier F, Richon P. 2006b. Thermal stratification induced by heating in a non-adiabatic context. Building and Environment 41:926-939.

Gao CF, Lee WL. 2011. Evaluating the influence of openings configuration on natural ventilation performance of residential units in Hong Kong. Building and Environment 46:961-969.

Hayashi T, Ishizu Y, Kato S, Murakami S. 2002. CFD analysis on characteristics of contaminated indoor air ventilation and its application in the evaluation of the effects of contaminant inhalation by a human occupant. Building and Environment 37:219-230.

Howell SA, Potts I. 2002. On the natural displacement flow through a full-scale enclosure, and the importance of the radiative participation of

the water vapour content of the ambient air. Building and Environment 37:817-823.

Hussain S, Oosthuizen PH. 2012. Validation of numerical modeling of conditions in an atrium space with a hybrid ventilation system. Building and Environment 52:152-161.

Hussain S, Oosthuizen PH, Kalendar A. 2012. Evaluation of various turbulence models for the prediction of the airflow and temperature distributions in atria. Energy and Buildings 48:18-28.

ISO. 2007. Building components and building elements - Thermal resistance and thermal transmittance - Calculation method (ISO 6946:2007), Second ed.

Launder BE, Spalding DB. 1972. Lectures in mathematical models of turbulence. London, England: Academic Press.

Li Y. 2000. Buoyancy-driven natural ventilation in a thermally stratified one-zone building. Building and Environment 35:207-214.

Li Y, Sandberg M, Fuchs L. 1992. Vertical temperature profiles in rooms ventilated by displacement: Full-scale measurement and nodal modelling. Indoor Air 2:225-243.

Li Y, Sandberg M, Fuchs L. 1993. Effects of thermal radiation on airflow with displacement ventilation: an experimental investigation. Energy and Buildings 19:263-274.

Linden PF. 1999. The fluid mechanics of natural ventilation. Annual Review of Fluid Mechanics 31:201-238.

Menter FR. 1994. Two-equation eddy-viscosity turbulence models for engineering applications. AIAA Journal 32:1598-1605.

Nielsen PV, Restivo A, Whitelaw JH. 1979. Buoyancy-affected flows in ventilated rooms. Numerical Heat Transfer, Part A 2:115-127.

Ramponi R, Blocken B. 2012. CFD simulation of cross-ventilation for a generic isolated building: Impact of computational parameters. Building and Environment 53:34-48.

Roache PJ. 1994. Perspective: A method for uniform reporting of grid refinement studies. Journal of Fluids Engineering 116:405-413.

Roache PJ. 1997. Quantification of uncertainty in computational fluid dynamics. Annual Review of Fluid Mechanics 29:123-160.

Saïd MNA, MacDonald RA, Durrant GC. 1996. Measurement of thermal stratification in large single-cell buildings. Energy and Buildings 24:105-115.

Shih T-H, Liou WW, Shabbir A, Yang Z, Zhu J. 1995. A new k-ε eddy viscosity model for high reynolds number turbulent flows. Computers and Fluids 24:227-238.

Stamou A, Katsiris I. 2006. Verification of a CFD model for indoor airflow and heat transfer. Building and Environment 41:1171-1181.

Tovar R, Linden PF, Thomas LP. 2007. Hybrid ventilation in two interconnected rooms with a buoyancy source. Solar Energy 81:683-691.

van Hooff T, Blocken B. 2010. Coupled urban wind flow and indoor natural ventilation modelling on a high-resolution grid: A case study for the Amsterdam ArenA stadium. Environmental Modelling and Software 25:51-65.

Wan MP, Chao CY. 2005. Numerical and experimental study of velocity and temperature characteristics in a ventilated enclosure with underfloor ventilation systems. Indoor Air 15:342-355.

Wilcox DC. 1998. Turbulence modeling for CFD. La Canada, California: DCW Industries, Inc.

Wolfshtein M. 1969. The velocity and temperature distribution in one-dimensional flow with turbulence augmentation and pressure gradient. International Journal of Heat and Mass Transfer 12:301-318.

Xu M, Yamanaka T, Kotani H. 2001. Vertical profiles of temperature and contaminant concentration in rooms ventilated by displacement with heat loss through room envelopes. Indoor Air 11:111-119.

Yakhot V, Orszag S. 1986. Renormalization group analysis of turbulence. I. Basic theory. Journal of Scientific Computing 1:3-51.

Table 1 measured interior surface temperature of vertical walls at different heights

HEIGHT (z) [m]	TEMPERATURE [K]
0.08	295.59
0.73	296.58
1.39	297.17
2.04	297.67
2.68	297.58

Table 2 defined interior surface temperature of vertical walls at different heights

HEIGHT (z) [m]	TEMPERATURE [K]
$0.00 \leq z < 0.08$	(z - 16.13)/(-0.05)
$0.08 \leq z < 0.73$	(z + 195.44)/(0.66)
$0.73 \leq z < 1.39$	(z + 333.89)/(1.13)
$1.39 \leq z < 2.04$	(z + 377.94)/(1.28)
$2.04 \leq z < 2.68$	(z - 2114.17)/(-7.10)
$2.68 \leq z \leq 2.75$	(z - 88.80)/(-0.29)

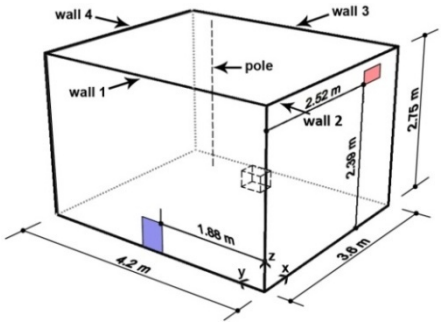

Figure 1 Geometry of the test-room, along with the position of the inlet and outlet openings and the heat source

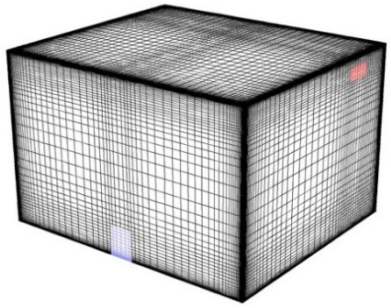

Figure 2 High-resolution computational grid (451,248 cells)

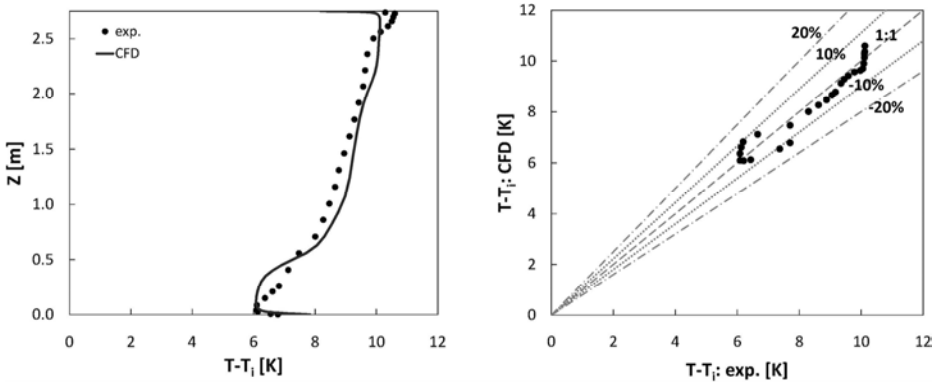

Figure 3 (a) Comparison of temperature difference (T –T_i) by CFD simulation results and experiment, (b) absolute deviation along the vertical pole

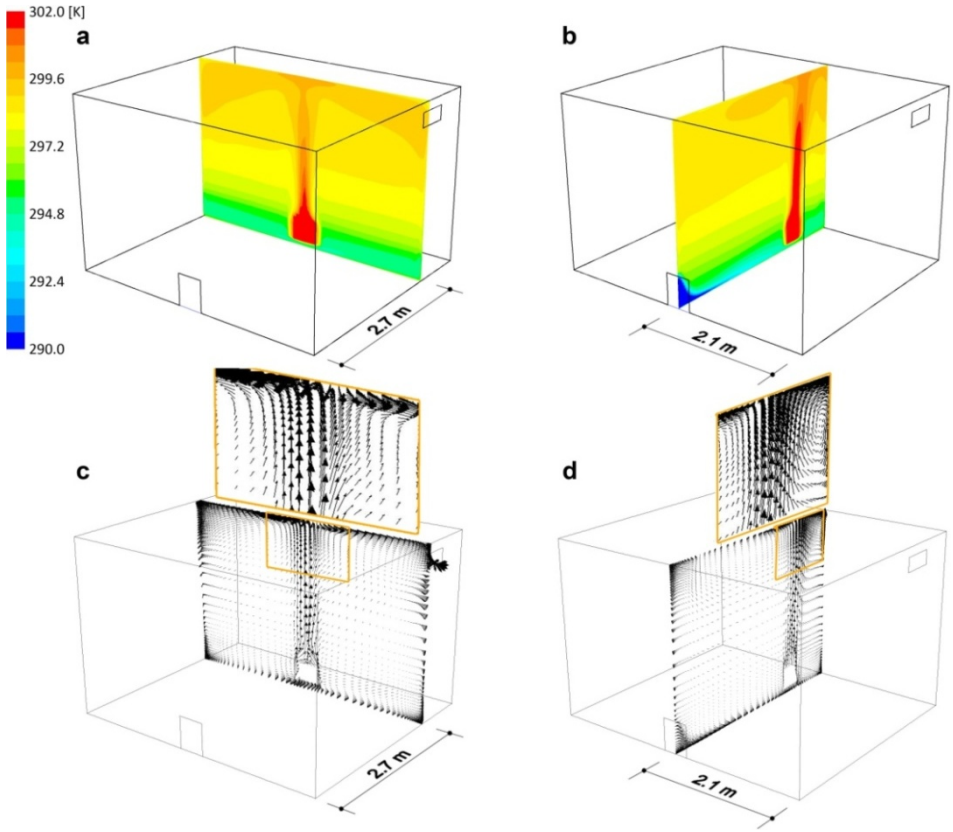

Figure 4 (a, b) Air temperature distribution, (c, d) velocity vector field across two vertical planes

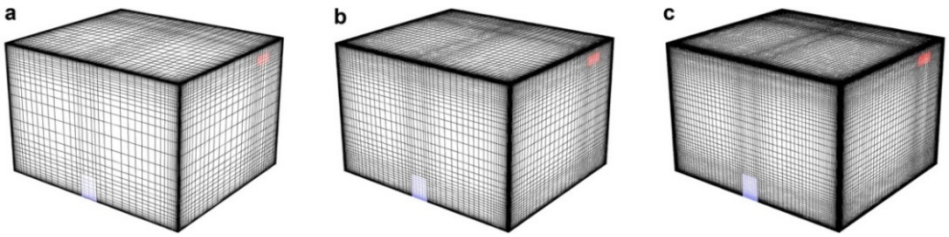

Figure 5 Computational grids for grid-sensitivity analysis: (a) coarse grid (155,382 cells), (b) reference grid (451,248 cells), (c) fine grid (1,268,736 cells)

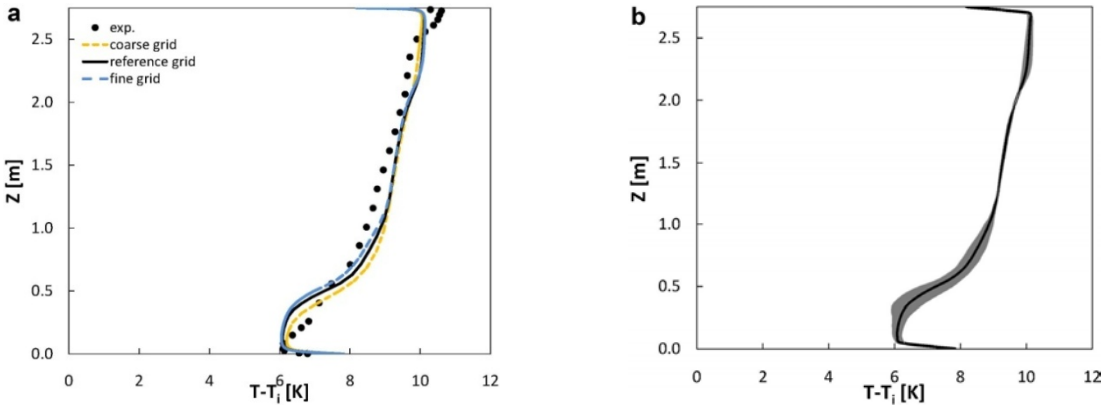

Figure 6 Impact of the grid resolution on temperature difference along the vertical pole: (a) comparison of results from the three grids , (b) results on reference grid with error band of GCI = 1.25 × Richardson Extrapolation error estimator by Roache (1994, 1997)

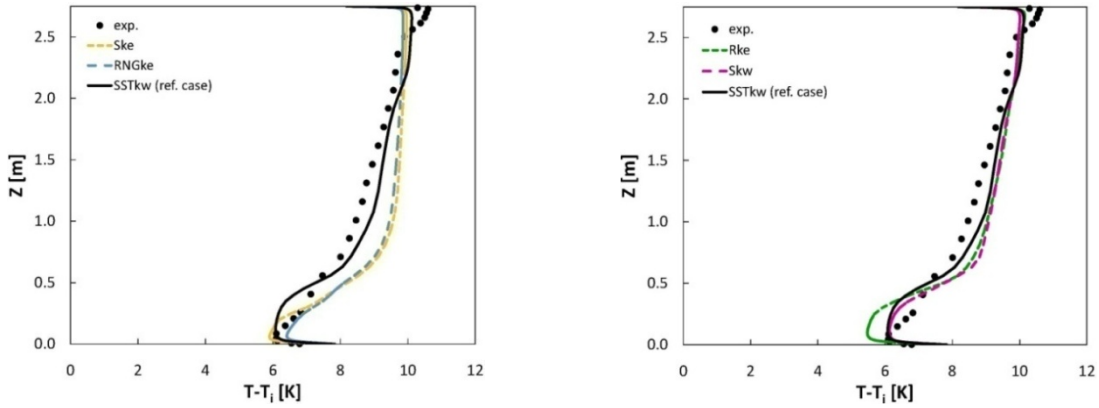

Figure 7 Impact of the turbulence models on CFD simulation results of temperature difference along the vertical pole

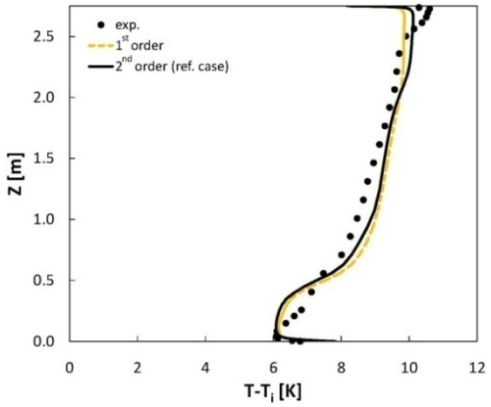

Figure 8 Impact of the discretization scheme on temperature difference along the vertical pole

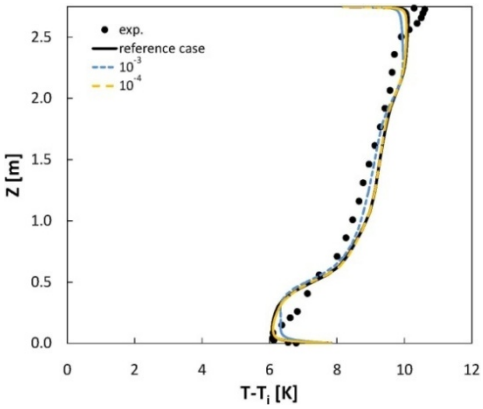

Figure 9 Impact of the iterative convergence limit on temperature difference along the vertical pole